Balogh-Michels et al. Journal of the European Optical Society-Rapid Publications (2021) 17:3
https://doi.org/10.1186/s41476-021-00147-w

Journal of the European Optical Society-Rapid Publications

RESEARCH Open Access

Crystallization behavior of ion beam sputtered HfO_2 thin films and its effect on the laser-induced damage threshold

Zoltán Balogh-Michels[1,2*], Igor Stevanovic[1], Aurelio Borzi[2], Andreas Bächli[1], Daniel Schachtler[1], Thomas Gischkat[1], Antonia Neels[2], Alexander Stuck[1] and Roelene Botha[1]

Abstract

In this work, we present our results about the thermal crystallization of ion beam sputtered hafnia on 0001 SiO_2 substrates and its effect on the laser-induced damage threshold (LIDT). The crystallization process was studied using in-situ X-ray diffractometry. We determined an activation energy for crystallization of 2.6 ± 0.5 eV. It was found that the growth of the crystallites follows a two-dimensional growth mode. This, in combination with the high activation energy, leads to an apparent layer thickness-dependent crystallization temperature. LIDT measurements @355 nm on thermally treated 3 quarter-wave thick hafnia layers show a decrement of the 0% LIDT for 1 h @773 K treatment. Thermal treatment for 5 h leads to a significant increment of the LIDT values.

Keywords: Hafnia, Grain growth, Crystallization, Thin films, X-ray diffraction, Laser-induced damage threshold

Introduction

Thin-film interference coatings, like antireflection or high reflectance coatings as well as wavelength and polarization selective coatings, are key elements of optical components as they allow to tune or even radically alter their optical properties [1, 2]. Ion beam sputtered (IBS) multilayers represent the current high-end optical coatings in the VIS/NIR range. Compared to other optical coating techniques, the sputtered atoms have high surface mobility due to their high energies (> 10 eV). Consequently, thin films by means of IBS are amorphous and provide the lowest surface roughness and lowest defect concentration for optical applications [3]. Furthermore, light scattering due to the grain boundaries is avoided in the amorphous film structure. Contemporary IBS allows manufacturing high reflective mirror coatings with optical losses below 1 ppm at a wavelength of 643 nm [4]. In laser applications, SiO_2 and HfO_2 are preferred in the multilayer stack as low and high refractive index material, respectively. Besides low optical losses, low absorption in the UV range, HfO_2 exhibits a high laser-induced damage threshold compared to other high index materials [5–7].

However, future applications, like new gravitational wave detectors [8, 9] or more precise optical clocks [10], require even smaller optical losses. The primary source of the losses in amorphous mirrors is the Brownian motion of the atoms [8, 11]. Current possibilities of circumventing the problem of the Brownian losses are by active cooling during operation e.g. [12], which is neither very efficient nor simple or straightforward. Single crystalline coatings instead of amorphous coatings can achieve an inherent reduction of Brownian loss. This was already shown for optical coatings working in the infrared range by applying epitaxial grown $GaAs/Al_xGa_{1-x}As$ multilayers and a subsequent substrate transfer [13–15].

By the fact that no matching substrates exist for the typical coating layers (e.g. HfO_2/SiO_2, Ta_2O_5/SiO_2), this method is not applicable for coatings in the visible range. To enable applications, which requires single

* Correspondence: zoltan.balogh@rhysearch.ch
[1]RhySearch, Werdenbergstrasse 4, CH9471 Buchs, SG, Switzerland
[2]Center for X-ray Analytics, Empa, Überlandstrasse 129, CH8600 Dübendorf, Switzerland

Springer Open

© The Author(s). 2021 **Open Access** This article is licensed under a Creative Commons Attribution 4.0 International License, which permits use, sharing, adaptation, distribution and reproduction in any medium or format, as long as you give appropriate credit to the original author(s) and the source, provide a link to the Creative Commons licence, and indicate if changes were made. The images or other third party material in this article are included in the article's Creative Commons licence, unless indicated otherwise in a credit line to the material. If material is not included in the article's Creative Commons licence and your intended use is not permitted by statutory regulation or exceeds the permitted use, you will need to obtain permission directly from the copyright holder. To view a copy of this licence, visit http://creativecommons.org/licenses/by/4.0/.

crystalline coatings in the visible range, it is essential to gain knowledge on non-epitaxial crystallization to tailor the process.

Thus, the material and its phase transitions have attracted research interest in the past decades since it also promises high-k dielectric for semiconductor applications. A few reports on the crystallization of hafnia on Si substrates exist. These include thermal crystallization of amorphous oxides [16], thermal oxidation of metallic hafnium [17], observation of spontaneous crystallization during atomic layer deposition (ALD) [18, 19], the layer thickness [20] or composition dependence of the crystallization temperature [21] and even an attempt to crystallize the hafnia using laser irradiation [22]. Liu et al. investigated the effect of heat treatment on thick IBS hafnia layers deposited on fused silica and single crystalline silicon substrates and reported a stress reduction accompanying the partial crystallization [23]. A recent publication by Abromavicius et al. [24] revealed that crystallization of IBS-HfO_2 can lead to higher LIDT due to stress reduction and/or better thermal management.

Experimental details

Crystallization

The coating was done by reactive IBS from a metallic Hf-target (Plasmaterials with 3 N purity) using a Veeco Spector 1.5 Dual Ion Beam Sputter (DIBS) instrument. The substrates for XRD measurements were epi-polished $10 \times 10\,mm^2$ SiO_2 single crystals with 0001 orientation from CrysTec. Prior to coating, the samples were in-situ treated with energetic O_2 ions (1 keV) for 10 min using the second plasma source of the Veeco DIBS machine.

To achieve complete oxidization, the target was flooded with 35 ccm O_2 during the target cleaning and the sputtering sequence. To investigate thickness dependence of the crystallization, we deposited 10, 15, 20, and 50 nm thick HfO_2 layers on the substrate. We determined the sputter rate using an ex-situ profilometer measurement.

The in-situ XRD annealing experiments were carried out using a Bruker D8 Discovery DaVinci diffractometer. The X-ray beam from a standard Cu Kα source (in this experiment λ = 1.5418 Å) is parallelized in the scattering plane by a Goebel mirror and detected by a LynxEye 1D detector. Since polycrystalline films were expected, we selected a grazing incidence geometry, with ω = 2° as an incoming angle. The 2θ range was 28–35°, which contained the expected main peaks of both the cubic and monoclinic HfO_2 [17]. The single crystalline SiO_2 substrates are zero-background substrates for this method, in contrast to the common fused silica.

The in-situ measurements were carried out using an Anton Paar DHS1100 high-temperature stage. We carried out an isochronal annealing sequence to gain an overall view of the transformation with 50 K steps and a holding time of 30 min using a 10 nm thick specimen. Based on this information, we performed isothermal scans with temperatures between 823 and 923 K using the 15 to 50 nm thick samples. The period between each single scan was 6 min. The scans were repeated until no significant change in the XRD pattern was observed in a few subsequent scans.

Figure 1 shows the cubic (111) HfO2 peak's proximity in a typical scan (50 nm thick layer, 823 K, 30 min). To integrate the peaks, the background was deduced by a simple linear function approximation, marked by a gray line in Fig. 1. From the peak areas, the transformed fraction f (normalized peak area) was calculated and later fitted as a function of the time t in accordance to the JMAK-equation [25]:

$$f = 1 - \exp\left(-\left(\frac{t}{t_c}\right)^{1+n'}\right), \tag{1}$$

with the two fitting parameters: $1 + n'$ and t_c. Hereby the well-known Avrami-exponent containing information on the nucleation and the growth is presented in $1 + n'$ form. Assuming a constant nucleation rate, the exponent n' is the dimensionality of the growth, e.g. $n' = 3$ means three dimensional or volumetric growth, while $n' = 2$ means two dimensional or film like growth. The t_c factor is the crystallization time, which can be derived from the N nucleation and G growth rate:

$$t_c \sim \left(NG^{n'}\right)^{-\frac{1}{n'+1}}. \tag{2}$$

Rewriting Eq. (1) into:

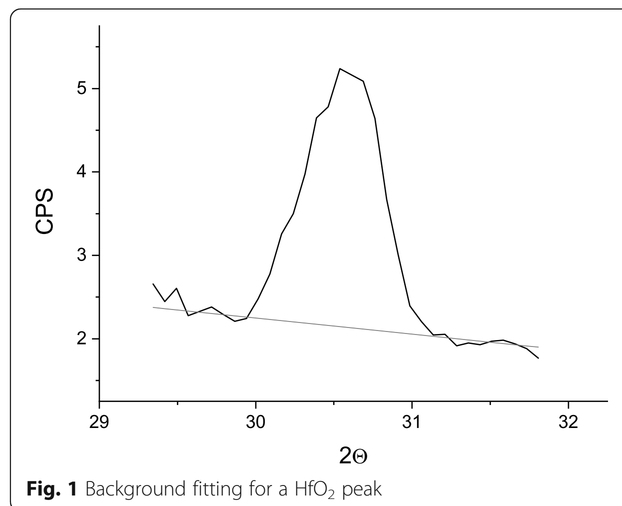

Fig. 1 Background fitting for a HfO_2 peak

$$\ln(-\ln(1-f)) = (1+n')\ln t - \ln t_c, \quad (3)$$

a linear fit can be performed to determine the parameters t_c and n'. This fitting strategy is more sensitive in the detection of changes in the dimensionality. To verify the measurements' consistency, the raw data and the fitting function were also compared with the transformed function vs. time scale (e.g. Eq. 1).

To estimate the activation energies of the crystallization, an Arrhenius-plot was performed according to:

$$t_c(T,d) = t_{0,d}\exp\left(\frac{Q}{k_B T}\right), \quad (4)$$

where the t_c is dependent of the temperature T and the layer thickness d, $t_{0,d}$ is a layer thickness dependent pre-factor, Q is the layer thickness independent activation energy, and k_B is the Boltzmann-constant.

Finally, we investigated the sample surfaces in their as-deposited and annealed state using a Veeco Dimension 3100 atomic force microscope (AFM).

Laser-damage testing

For the LIDT measurements, we used P4 polished (rms roughness of about 3 Å, scratch-dig 20–10) fused silica substrates provided by WZW Optics AG. We chose a layer thickness of 3 quarter-wave @355 nm, which ensured an electric field maxima in the layer itself. We produced three sets of specimens; the first set was left in the as-prepared state ("amorphous"), the second one we annealed at 773 K for 1 h ("intermediate"), while the last set was annealed for 5 h at 773 K ("crystalline").

Laser-damage testing was performed using a Litron LPYG-450-100 diode-pumped laser at 355 nm [26]. The repetition rate was 100 Hz, while the pulse duration was 11.6 ns. The effective beam diameter, calculated according to ISO 21254-1:2011 [27], at the surface was 230 μm. The specimens were acclimatized for 24 h before the experiments in the laboratory (20 °C temperature, < 50% relative humidity). We carried out S-on-1 measurements with S = 5000. At least 150 sites were irradiated with appropriately chosen laser fluences. We performed the well-known but non-ISO conform test data reduction according to Jensen et al. [28] to improve the data quality in the relevant regime.

We used a scattered light detector to identify the first damage. To verify the detected damage events, a visual inspection through a differential interference contrast microscopy (Leica DM4000 M Led) was performed.

According to the ISO norm 21,254 [27], for each test site, there are three pieces of information: 1.) whether the site is damaged (1/0), 2.) the applied laser fluence Q, and 3.) the number of pulses applied before the damage onset N_{min}. If no damage took place, this value is S. The derived data is the probability of damage by a given combination of $Q \pm \Delta Q$ fluence interval and N pulse number. A site is considered damaged if

$$\begin{Bmatrix} N > N_{min} & 1 \\ N \leq N_{min} & 0 \end{Bmatrix} \quad (5)$$

The cumulative test method [28] assumes that if an experiment with any fluence of Q' > Q and N_{min} pulses damage would also have been observed.

There are different interpretations of the data. We chose the following two: 1.) the characteristic damage curve or the probability of damage if S pulses are applied at a given fluence 2.) the damage probability as a function of the fluence a given number of pulses.

The specimens used in the laser-damage testing were also checked in ex-situ measurements for their crystallinity using a PanAlytical Empyrean X-ray diffractometer. This system is also equipped with a Cu Kα source. We applied two methods GIXRD at ω = 2° to identify the crystalline phases and X-ray reflectometry (XRR) to determine the density of the layers.

Results

Crystallization

The crystallization was first observed at 973 K for the 10 nm thick films, and the phase was identified to be cubic HfO_2. After increasing the temperature to 1273 K, a transformation to the stable monoclinic phase took place. We carried out room temperature ex-situ measurements with slow scan speeds for a better signal-to-noise ratio. These scans are shown in Fig. 2.

Since the intensity of the peaks for 10 nm thick layers were not high enough for reliable kinetics experiments, we studied the crystallization kinetics only of the 15–50

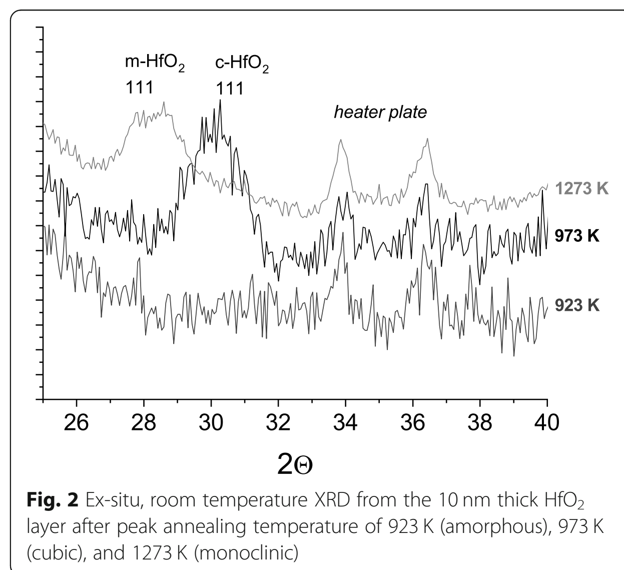

Fig. 2 Ex-situ, room temperature XRD from the 10 nm thick HfO_2 layer after peak annealing temperature of 923 K (amorphous), 973 K (cubic), and 1273 K (monoclinic)

nm thick films. Figure 3a shows an example of such kinetics: the development of the cubic (111) peak for the 50 nm thick HfO_2 film annealed at 823 K.

In Fig. 3b, the measured and the fitted transferred fraction as a function of time are shown for the 50 nm HfO_2 film. The small insert gives the logarithmic plot in accordance to Eq. (3). The fitting function is in good agreement with the measured data both in the linear and logarithmic scale. The *n*' exponent, in this case, is 2.15 ± 0.1 for this experiment, and no deviation from this behavior is visible in the early stages. The transformation for the 50 nm film took place at a much lower temperature than for the 10 nm thick film.

Table 1 summarizes the crystallization times for the different temperatures and the corresponding dimensionality of the growth *n*' for the different investigated film thicknesses. For some experiments, the crystallization was too fast. Consequently, only an upper limit of the crystallization time can be given in these cases. We evaluated the exponent *n*' only where the amount of data could provide a reliable fitting.

Table 1 The evaluation of the experiments

Thickness (nm)	Temp (K)	Cryst time (min)	n'
10	973	~ 30	–
15	873	8	–
15	858	16	2.05
15	843	55	1.85
20	923	< 2	–
20	873	6	–
20	843	24	2.05
50	843	8	–
50	823	45	2.15

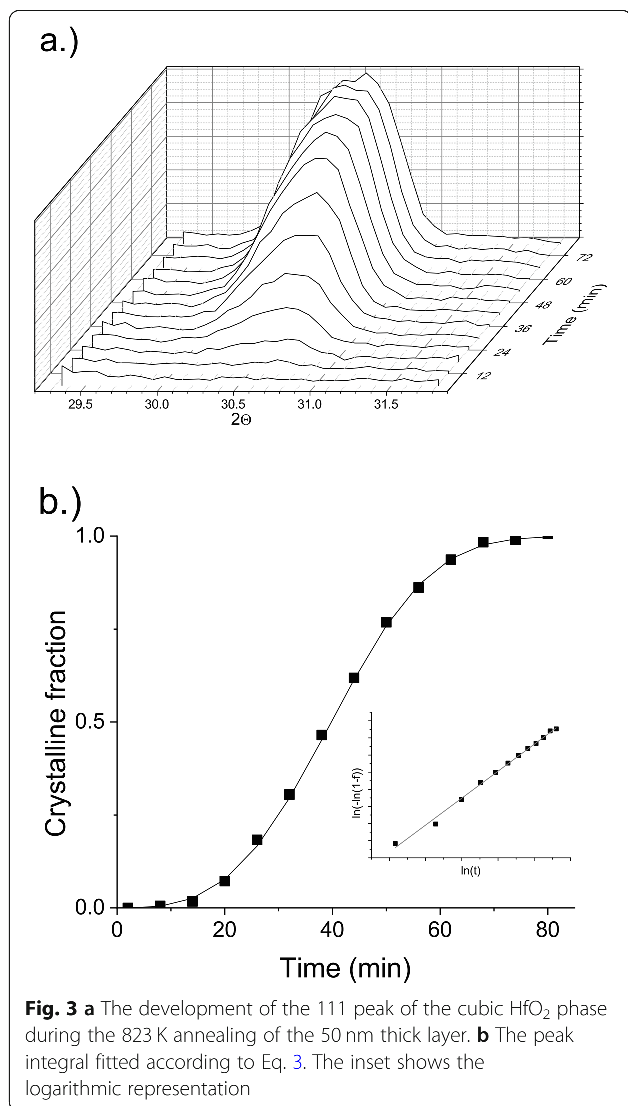

Fig. 3 **a** The development of the 111 peak of the cubic HfO_2 phase during the 823 K annealing of the 50 nm thick layer. **b** The peak integral fitted according to Eq. 3. The inset shows the logarithmic representation

Laser-damage testing

To gain information on the crystallinity state of the sample GIXRD was performed on the samples used in the laser damage test. Figure 4 shows the results of these

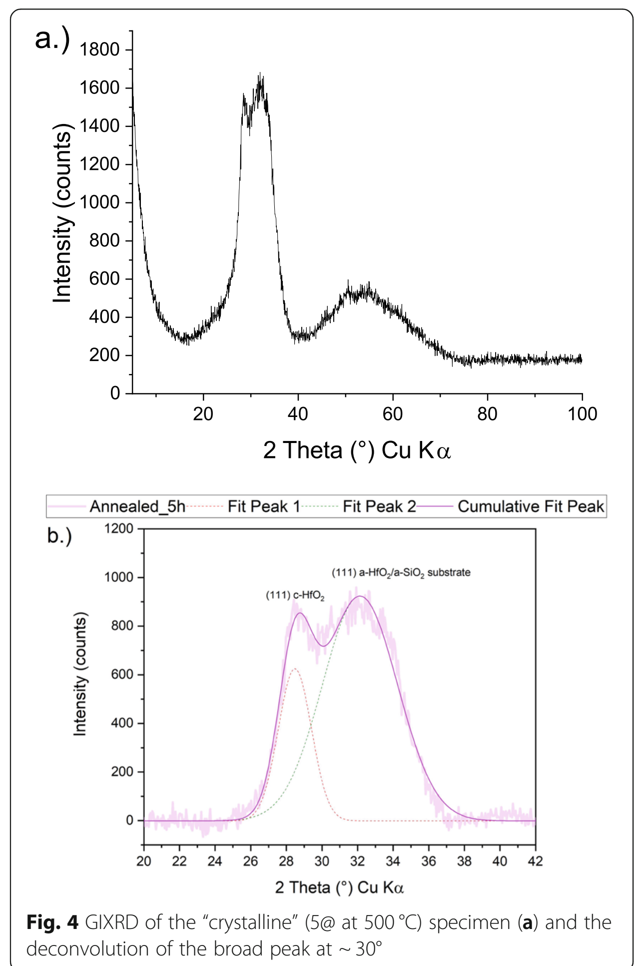

Fig. 4 GIXRD of the "crystalline" (5@ at 500 °C) specimen (**a**) and the deconvolution of the broad peak at ~ 30°

Table 2 Crystallization parameters of the specimens

Specimen name	Annealing treatment	Area: c-HfO_2 to amorphous	Scherrer-size (nm)	Density (gcm^{-3})
Amorphous	n.a	0	n.a	9.29
Intermediate	1 h @ 500 °C	0.22 ± 0.02	1.5	8.86
Crystalline	5 h @ 500 °C	0.30 ± 0.01	1.9	8.78

GIXRD experiment for the 5 h annealed "crystalline" specimen. Fused silica is not an ideal substrate for such investigations since the broad peak centered around 32° could belong to either SiO_2 or HfO_2. Nevertheless, the much sharper c-HfO_2 peak could be separated and characterized (Fig. 4b). Table 2 shows the results of GIXRD and XRR experiments: the ratio of the peak area of the c-HfO2 to the amorphous peak, the Scherrer-size of the crystallites, and the layer density.

Figure 5 shows the results of the LIDT experiments using two interpretations. In Fig. 5a, the damage probability (N = 5000) is plotted as a function of the pulse energies for the different specimens. In Fig. 5b, the 5% LIDT is plotted against the number of pulses.

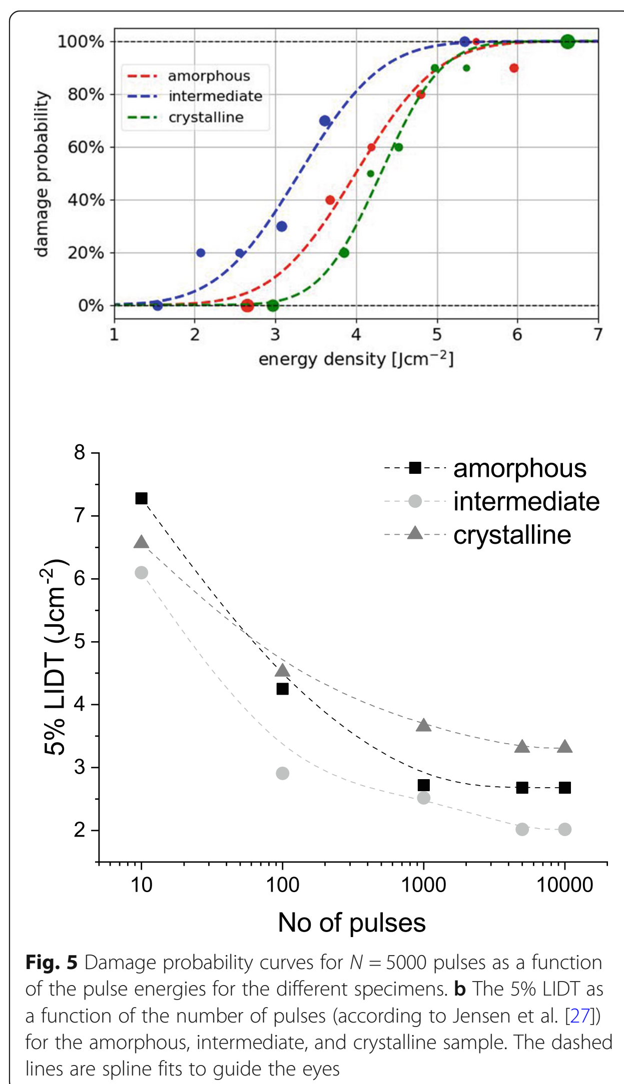

Fig. 5 Damage probability curves for N = 5000 pulses as a function of the pulse energies for the different specimens. **b** The 5% LIDT as a function of the number of pulses (according to Jensen et al. [27]) for the amorphous, intermediate, and crystalline sample. The dashed lines are spline fits to guide the eyes

It can clearly be seen from Fig. 5a that the "crystalline" specimen has the highest damage onset, highest 0% LIDT and its 100% LIDT is not worse than that of the "amorphous" specimen. Surprisingly the "intermediate" specimen produced the worst result.

A similar trend can be seen for the 5% LIDT curves. The "crystalline" specimen shows higher laser-damage resistance for all but the lowest number of laser pulses than the "amorphous" one. On the other hand, the "intermediate" specimens show consequently the worst 5% LIDT values. The differences are larger than the expected measurement scatter.

Discussion

Crystallization

As it can be seen in Table 1, crystallization experiments performed on the 15, 20, and 50 nm thick films provided exponents of about 2, which indicates a two-dimensional growth. This shows that the distances between different nucleation centers are larger than the 50 nm film thickness.

This is supported by the findings of the atomic AFM measurements shown in Fig. 6. Figure 6a shows the AFM of the 50 nm HfO_2 coated sample before while Fig. 6b shows a specimen after the thermal treatment. The smooth surface (RMS roughness 0.26 nm) of the as deposited sample changes to structured surface with a RMS roughness of about 0.65 nm. The needlelike and triangular structures with a few hundreds of nanometers lateral dimensions and 5–10 nm height have a mean distance in the micrometer range.

In Fig. 7, all crystallization times are plotted as a function of the inverse temperature. The depicted lines are the fitted Arrhenius-type functions.

The average activation energy turned out to be 2.6 ± 0.5 eV, while the prefactors for the 50, 20, and 15 nm layers are respectively 5.8×10^{-14} s, 8.4×10^{-14} s, and 1.7×10^{-13} s. This ratio of 1:1.5:3 is comparable to the layer thicknesses. Thus, in our experiment, the layer thickness dependence is probably a consequence of the crystallization's two-dimensional nature. For this situation, the nucleation rate per area and not per volume is decisive for the transformation rate. For a thinner film, even for equal volumetric nucleation rate, there is a much-reduced number of nuclei per area.

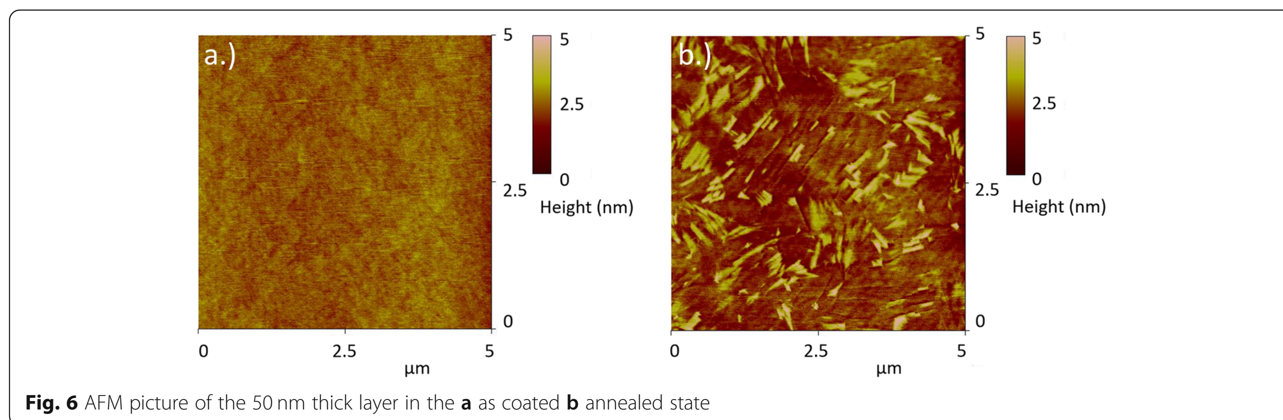

Fig. 6 AFM picture of the 50 nm thick layer in the **a** as coated **b** annealed state

In general, crystallization is getting easier with an increasing layer thickness, even though our layers are much thicker than the 1.5–5 nm critical thickness reported by Nie et al. [20].

According to Eqs. (1–3), the transformed volume fraction is dominated by the growth term even for two-dimensional growth modes. Short and long-range atomic jumps i.e. diffusion is a thermally activated rate-controlling process which usually plays a crucial role in crystallite growth. Since hafnia has two sublattices it is interesting whether the cation or the anion jumps are controlling the crystallization.

The activation energy of 2.6 ± 0.5 eV is much higher than the reported experimental activation energy of 1 eV for oxygen self-diffusion in monoclinic hafnia [29]. Some theoretical reports [30, 31] assume even lower oxygen activation energies.

We found no report on the self-diffusion of Hf in the different HfO_2 phases. However, ZrO_2 phases have almost identical lattice parameters as the respective HfO_2 phases. Thus, it is often used for comparisons. An experimental series by Swaroop et al. [32] to compare the diffusivity of different cations in yttria-stabilized tetragonal zirconia has shown that Hf′s activation energy is virtually identical to that of the Zr (5.3 eV for lattice and 3.8 eV for grain boundary diffusion).

Computational studies e.g. Refs [33, 34] on the Zr self-diffusion lead to an activation energy well above that of the oxygen's (2.5 eV or higher). During the sintering of ZrO_2 particles, Suárez et al. found that the activation energy of Zr self-diffusion in ZrO_2 is 2.3 eV. Furthermore, they also reported that it is the Zr self-diffusion, which controls the sintering process [35]. Our activation energy of 2.6 ± 0.5 eV is comparable to that of the cation diffusion in ZrO_2. Therefore, cation atomic jumps could play a more important role in the crystallization of HfO_2 films.

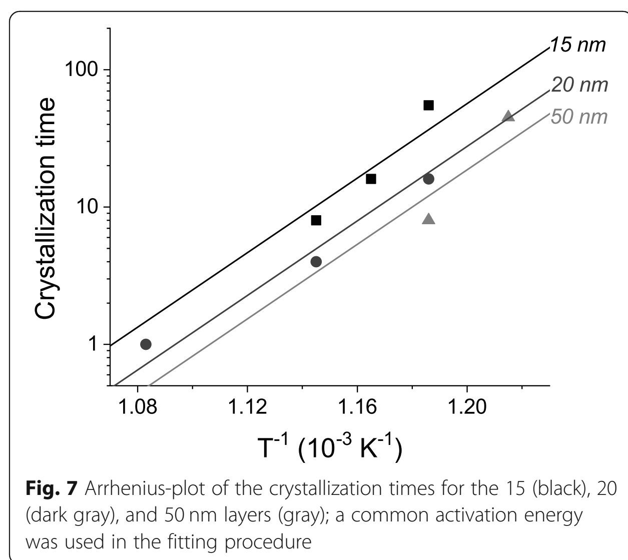

Fig. 7 Arrhenius-plot of the crystallization times for the 15 (black), 20 (dark gray), and 50 nm layers (gray); a common activation energy was used in the fitting procedure

Laser-damage testing

Thermal treatment to cure defects and/or reduce stress levels is a well-known method for improving the laser-damage threshold (e.g. [23, 24, 36, 37]). However, typical annealing treatments stay well below the crystallization limits, as the presence of grain boundaries leads to an increase in the scattered light.

Nevertheless, in the case of hafnia, it is also proven that crystallization [24] is an efficient method of increasing the single layer LIDT and multilayer coatings. Our results for the long annealing times are in qualitative agreement with this finding. We did not observe the very prominent increase of the LIDT as reported in [24], which is not surprising as we annealed at a lower temperature of 500 °C instead of the 600 and 700 °C marked as the optimal “high-temperature” annealing by Abromavicius et al. Indeed the observed Scherrer-size indicates that HfO_2 crystallites are either very small or they are highly strained [38]. Irrespective of the origin of

the line-broadening, the layers did not reach a relaxed, coarse-grained state.

We also found an intermediate decrement of the LIDT values, which is not reported in [24] and worth further investigation. One explanation for the small Scherrer-size is high stress, this according to our own experience leads to low LIDT [39]. The other possibility is a high concentration of grain boundaries, which according to Tateno et al. [40] can also be a cause for reduced LIDT. Due to the higher temperatures, no comparable specimen was present in Ref. [24], which could explain why we observed a reduction of the LIDT.

Conclusion

We analyzed the crystallization kinetics of IBS deposited HfO_2 via in-situ XRD. We found that the crystallization for thin films up to 50 nm thickness follows the two-dimensional growth mode. The activation energy of the crystallization kinetics is 2.6 ± 0.5 eV which indicates that the displacement of Hf atoms could play a rate controlling role in the crystallization.

We have proven that crystallization leads to a higher LIDT value. However, we also found that a decrement of the laser-damage resistance takes place at an intermediate stage.

Acknowledgments

The authors thank Dr. Marlies Höland for the contributions to the experimental results.

Authors' contributions

Z. Balogh-Michels: data acquisition, interpretation, design of work, original draft; I. Stevanovic: data acquisition; A. Borzi: data acquisition, interpretation, A. Bächli: conception of work, revision of draft; D. Schachtler: data acquisition, interpretation; T. Gischkat: conception of work, design of work, interpretation, revision of draft; A. Neels: design of work, data interpretation; A. Stuck: conception of work, design of work; R. Botha: conception of work. The author(s) read and approved the final manuscript.

Funding

We would like to thank the Swiss Canton of St. Gallen and the Principality of Liechtenstein for supporting RhySearch.

Availability of data and materials

The datasets used and/or analysed during the current study are available from the corresponding author on reasonable request.

Declarations

Competing interests

The authors declare that they have no competing interests.

Received: 21 December 2020 Accepted: 21 February 2021
Published online: 06 March 2021

References

1. Kaiser, N., Pulker, H.K.: Optical Interference Coatings. Springer Verlag, Berlin (2003)
2. Ristau, D.: Laser-Induced Damage in Optical Materials. CRC Press, Boca Raton, FL (USA), 2015 ISBN: 978-1-4398-7217-8
3. Langdon, B., Patel, D., Krous, E., Rocca, J.J., Menoni, C.S., Tomasel, F., Kholi, S., McCurdy, P.R., Langston, P., Ogloza, A.: Influence of process conditions on the optical properties of HfO2/SiO2 coatings for high-power laser coatings. Proc. SPIE. **6720**, 67200X (2007). https://doi.org/10.1117/12.753027
4. Rempe, G., Thompson, R.J., Kimble, H.J., Lalezari, R.: Measurement of ultralow losses in an optical interferometer. Opt. Lett. **17**, 363 (1992). https://doi.org/10.1364/OL.17.000363
5. Alvisi, M., Di Giulio, M., Marrone, S.G., Perrone, M.R., Protopapa, M.L., Valentini, A., Vasanelli, L.: HfO_2 films with high laser damage threshold. Thin Solid Films. **358**, 250 (2000). https://doi.org/10.1016/S0040-6090(99)00690-2
6. Akhtar, S.M.J., Ristau, D., Ebert, J., Welling, H.: High damage threshold single and double layer antireflection (AR) coating for Nd:YAG Laser: conventional systems. J. Optoelectron. Adv. Mater. **9**, 2391 (2007)
7. Stolz, C.J., Thomas, M.D., Griffin, A.J.: BDS thin film damage competition. Proc. SPIE. **7132**, 71320C (2008). https://doi.org/10.1117/12.806287
8. Miller, J., Barsotti, L., Vitale, S., Fritschel, P., Evans, M., Sigg, D.: Prospects for doubling the range of Advanced LIGO. Phys. Rev. D. **91**, 062005 (2015). https://doi.org/10.1103/PhysRevD.91.062005
9. Steinlechner, J.: Development of mirror coatings for gravitational wave detectors. Philos. Trans. R. Soc. A. **376**, 0282 (2018). https://doi.org/10.1098/rsta.2017.0282
10. Jiang, Y.Y., Ludlow, A.D., Lemke, N.D., Fox, R.W., Sherman, J.A., Ma, L.S., Oates, C.W.: Making optical atomic clocks more stable with 10-16-level laser stabilization. Nat. Photonics. **5**, 158 (2011). https://doi.org/10.1038/nphoton.2010.313
11. Harry, G., Bodiya, T., DeSalvo, R.: Optical Coatings and Thermal Noise in Precision Measurement. Cambridge University Press, Cambridge (UK), (2012) ISBN: 9781107003385
12. Aso, Y., Michimura, Y., Somiga, K., Ando, M., Miyakawa, O., Sekiguchi, T., Tatsumi, D., Yamamoto, H.: Interferometer design of the KAGRA gravitational wave detector. Phys. Rev. D. **88**, 043007 (2013). https://doi.org/10.1103/PhysRevD.88.043007
13. Cole, G.D., Zhang, W., Martin, M.J., Ye, J., Aspelmeyer, M.: Tenfold reduction of Brownian noise in high-reflective optical coatings. Nat. Photonics. **7**, 644 (2013). https://doi.org/10.1038/nphoton.2013.174
14. Cole, G.D., Zhang, W., Bjork, B.J., Follman, D., Heu, P., Deutsch, C., Sonderhouse, L., Robinson, J., Franz, C., Alexandrovski, A., Notcutt, M., Heckl, O.H., Ye, J., Aspelmeyer, M.: High performance near and mid-infrared crystalline coatings. Optica. **3**, 647 (2016). https://doi.org/10.1364/OPTICA.3.000647
15. Marchiò, M., Flaminio, R., Pinard, L., Forest, D., Deutsch, C., Heu, P., Follman, D., Cole, G.D.: Optical performance of large area crystalline coatings. Opt. Express. **5**, 6117 (2018). https://doi.org/10.1364/OE.26.006114
16. He, G., Liu, M., Zhu, L.Q., Chang, M., Fang, Q., Zhang, L.D.: Effect of postdeposition annealing on the thermal stability and structural characteristics of sputtered HfO_2 films on Si (100). Surf. Sci. **576**, 67 (2005). https://doi.org/10.1016/j.susc.2004.11.042
17. Xie, Y., Ma, Z., Su, Y., Liu, Y., Liu, L., Zhao, H., Zhou, J., Zhang, Z., Li, J., Xie, E.: The influence of mixed phases on optical properties of HfO2 thin films prepared by thermal oxidation. J. Mater. Res. **26**, 50 (2011). https://doi.org/10.1557/jmr.2010.61
18. Rammula, R., Aarik, J., Mänder, H., Ritslaid, P., Sammelselg, V.: Atomic layer deposition of HfO2: effect of structure development on growth rate, morphology and optical properties of thin films. Appl. Surf. Sci. **257**, 1043 (2010). https://doi.org/10.1016/j.apsusc.2010.07.105
19. Wei, Y., Xu, Q., Wang, Z., Liu, Z., Pan, F., Zhang, Q., Wang, J.: Growth properties and optical properties for HfO2 thin films deposited by atomic layer deposition. J. Alloys Cmpd. **738**, 1422 (2018). https://doi.org/10.1016/j.jallcom.2017.11.222
20. Nie, X., Ma, F., Ma, D.: Thermodynamics and kinetic behaviors of thickness-dependent crystallization in high-k thin films deposited by atomic layer deposition. J. Vacuum Sci. Technol. A. **33**, 01A140 (2015). https://doi.org/10.1116/1.4903946
21. Biswas, D., Singh, M.N., Sinha, A.K., Bhattacharyya, S., Chakraborty, S.: Effect of excess hafnium on HfO2 crystallization temperature and leakage current behavior of HfO2/Si metal-oxide semiconductor devices. J. Vacuum Sci. Tecnol. B. **34**, 022201 (2016). https://doi.org/10.1116/1.4941247
22. Kim, D.H., Park, J.W., Chang, Y.M., Lim, D., Chung, H.: Electrical properties and structure of laser-spike-annealed hafnium oxide. Thin Solid Films. **518**, 2812 (2010). https://doi.org/10.1016/j.tsf.2009.08.039
23. Liu, H., Jiang, Y., Wang, L., Li, S., Yang, X., Jiang, C., Liu, D., Ji, Y., Zhang, F., Chen, D.: Effect of heat tretament on properties of HfO2 film deposited by ion beam sputtering. Opt. Mater. **73**, 95 (2017). https://doi.org/10.1016/j.optmat.2017.07.048

24. Abromavicius, G., Kicas, S., Buzelis, R.: High temperature annealing effects on spectral, microstructural and laser damage resistance properties of sputtered HfO_2 and HfO_2-SiO_2 mixture-based UV mirrors. Opt. Mater. **95**, 109245 (2019). https://doi.org/10.1016/j.optmat.2019.109245
25. Avrami, M.: Kinetics of phase change. I general theory. J. Chem. Phys. **7**, 1103 (1939)
26. Gischkat, T., Schachtler, D., Balogh-Michels, Z., Botha, R., Mocker, A., Eiermann, B., Günther, S.: Influence of ultra-sonic frequency during substrate cleaning on the laser resistance of antireflection coatings. In: Proc. SPIE 11173, Laser-Induced Damage in Optical Materials, p. 1117317 (2019). https://doi.org/10.1117/12.2536442
27. ISO 21254-1:2011. International Organization for Standardization, Geneva. https://www.iso.org/standard/43001.html. Accessed 12 Nov 2018.
28. Jensen, L., Mrohs, M., Gyamfi, M., Mäderbach, H., Ristau, D.: Higher certainty of the laser-induced damage threshold testwith a redistributing data treatment. Rev. Sci. Instrum. **86**, 103106 (2015). https://doi.org/10.1063/1.4932617
29. Vos, M., Grande, P.L., Venkataalam, D.K., Nandi, S.K., Elliman, R.G.: Oxygen self-diffusion in HfO_2 studied by electron spectrography. Phys. Rev. Lett. **112**, 175901 (2014). https://doi.org/10.1103/PhysRevLett.112.175901
30. Capron, N.: Migration of oxygen vacancy in HfO_2 and across the HfO_2/SiO_2 interface: a first principle investigation. Appl. Phys. Lett. **91**, 192905 (2007). https://doi.org/10.1063/1.2807282
31. Shen, W., Kumari, N., Gibson, G., Jeon, Y., Henze, D., Silverthorn, S., Bash, C., Kumar, S.: Effect of annealing on structural changes and oxygen diffusion in amoprhous HfO2 using classical molecular dynamics. J. Appl. Phys. **123**, 085113 (2018). https://doi.org/10.1063/1.5009439
32. Swaroop, S., Kilo, M., Argirusis, C., Borchardt, G., Chokshi, A.H.: Lattice and grain boundary diffusion of cations in 3YTZ analyzed using SIMS. Acta Mater. **53**, 4975 (2005). https://doi.org/10.1016/j.actamat.2005.05.031
33. González-Romero, R.L., Meléndez, J.J., Gómez-García, D., Cumbrera, F.L., Domínguez-Rodríguez, A., Wakai, F.: Cation diffusion in yttria-zirconia by molecular dynamics. Solid State Ion. **204-205**, 1 (2011). https://doi.org/10.1016/j.ssi.2011.10.006
34. Dong, Y., Qi, L., Li, J., Chen, I.W.: A computational study of yttria-stabilized zirconia: II. Cation diffusion. Acta Mater. **126**, 438 (2017)
35. Suárez, G., Garrido, L.B., Aglietti, E.F.: Sintering kinetics of 8Y–cubic zirconia: Cation diffusion coefficient. Mater. Chem. Phys. **110**, 370 (2008). https://doi.org/10.1016/j.matchemphys.2008.02.021
36. Yao, J.K., Shao, H.D., He, H.B., Fan, Z.X.: Effects of annealing on laser-induced damage threshold of TiO_2/SiO_2 high reflectors. Appl. Surf. Sci. **253**, 8911–8914 (2007). https://doi.org/10.1016/j.apsusc.2007.05.005
37. Tan, T., Liu, Z., Lu, H., Liu, W., Tian, H.: Structure and optical properties of HfO2 thin films on silicon after rapid thermal annealing. Opt. Mater. **32**, 432–435 (2010). https://doi.org/10.1016/j.optmat.2009.10.003
38. Borzi, A., Dolabella, S., Szmyt, W., Geler-Kremer, J., Abel, S., Fompeyrine, J., Hoffmann, P., Neels, A.: Microstructure analysis of epitaxial $BaTiO_3$ thin films on $SrTiO_3$-buffered Si: Strain and dislocation density quantification using HRXRD methods. Materialia. **14**, 100953 (2020). https://doi.org/10.1016/j.mtla.2020.100953
39. Stevanovic, I., Balogh-Michels, Z., Bächli, A., Wittwer, V.J., Südmeyer, T., Stuck, A., Gischkat, T.: Influence of the secondary ion beam source on the laser damage mechanism and stress evolution of IBS hafnia layers. Appl. Sci. **11/1**, 189 (2021). https://doi.org/10.3390/app11010189
40. Tateno, R., Okada, H., Otobe, T., Kawase, K., Koga, J.K., Kosuge, A., Nagashima, K., Sugiyama, A., Kashiwagi, K.: Negative effect of crystallization on the mechanism of laser damage in a HfO_2/SiO_2 multilayer. J. Appl. Phys. **112**, 123103 (2012). https://doi.org/10.1063/1.4767231

Publisher's Note

Springer Nature remains neutral with regard to jurisdictional claims in published maps and institutional affiliations.

Submit your manuscript to a SpringerOpen journal and benefit from:

► Convenient online submission
► Rigorous peer review
► Open access: articles freely available online
► High visibility within the field
► Retaining the copyright to your article

Submit your next manuscript at ► springeropen.com